

A CLOSER LOOK AT THE LkCa 15 PROTOPLANETARY DISK

SEAN M. ANDREWS¹, KATHERINE A. ROSENFELD¹, DAVID J. WILNER¹, AND MICHAEL BREMER²

¹ Harvard-Smithsonian Center for Astrophysics, 60 Garden Street, Cambridge, MA 02138, USA

² IRAM, 300 Rue de la Piscine, F-38406 Saint Martin d’Hères, France

Received 2011 August 5; accepted 2011 October 6; published 2011 October 31

ABSTRACT

We present 870 μm observations of dust continuum emission from the LkCa 15 protoplanetary disk at high angular resolution (with a characteristic scale of $0''.25 = 35$ AU), obtained with the IRAM Plateau de Bure interferometer and supplemented by slightly lower resolution observations from the Submillimeter Array. We fit these data with simple morphological models to characterize the spectacular ring-like emission structure of this disk. Our analysis indicates that a small amount of 870 μm dust emission (~ 5 mJy) originates inside a large (40–50 AU radius) low optical depth cavity. This result can be interpreted either in the context of an abrupt decrease by a factor of ~ 5 in the radial distribution of millimeter-sized dust grains or as indirect evidence for a gap in the disk, in agreement with previous inferences from the unresolved infrared spectrum and scattered light images. A preliminary model focused on the latter possibility suggests the presence of a low-mass (planetary) companion, having properties commensurate with those inferred from the recent discovery of LkCa 15b.

Key words: circumstellar matter – planet–disk interactions – protoplanetary disks – stars: individual (LkCa 15) – submillimeter: planetary systems

Online-only material: color figures

1. INTRODUCTION

Hundreds of exoplanets have been discovered around main-sequence stars, and substantial effort is being invested to explain their demographics with formation models (e.g., Ida & Lin 2004; Mordasini et al. 2009). But associating exoplanet properties with their formation epoch is problematic: dramatic evolutionary processes that occur at early times are closely tied to the unknown physical conditions in the progenitor circumstellar disk. Ideally, mature exoplanets could be compared with their younger counterparts which are still embedded in their natal disks. However, detecting planets around young stars is difficult. Radial velocity and transit searches are hindered by stellar variability (e.g., Huélamo et al. 2008), and direct imaging is limited by contrast with the bright star and disk emission. However, the presence of a young planet can be inferred *indirectly* through its dynamical imprint on the structure of the disk material. A sufficiently massive planet ($\geq 1 M_{\text{Jup}}$) opens a gap that impedes the inward flow of mass through the disk, decreasing the densities at the disk center (e.g., Lin & Papaloizou 1986; Bryden et al. 1999; Quillen et al. 2004). The location of the gap marks the planet orbit, and the amount of material that flows across it depends on the planet mass (Lubow & D’Angelo 2006; Varnière et al. 2006). In principle, the orbit and mass of a \sim Myr-old giant planet can be estimated from observations of its disk birthsite, through constraints on the gap location and the amount of material interior to it, respectively.

The disk around the young star LkCa 15 is considered to be an excellent candidate for planet-induced disk clearing, based on its distinctive infrared spectrum (Espaillat et al. 2007) as well as the ring-like morphology of its millimeter-wave dust emission (Piétu et al. 2006; Andrews et al. 2011) and scattered light in the infrared (Thalmann et al. 2010). Those observations confirm that the LkCa 15 disk has a large central “cavity,” with significantly diminished dust optical depths on solar system size-scales. However, the cavity is not empty. A faint infrared signal is detected in excess of the stellar photosphere, indicating that at

least a small amount of warm dust resides near the star (Espaillat et al. 2008). That excess verifies the presence of a tenuous inner disk—and therefore a gap—although it provides only minimal bounds on its size (and therefore the gap width) and mass. Based on an attempt to model a high-resolution Submillimeter Array (SMA) observation of the LkCa 15 disk, Andrews et al. (2011) identified preliminary evidence for weak, optically thin 870 μm emission from dust *inside* the disk cavity. If confirmed, that emission can be used to estimate the inner disk mass, a key diagnostic of the flow rate across the gap.

In this Letter, we present new 870 μm continuum observations of the LkCa 15 protoplanetary disk, with a 50% improvement in angular resolution facilitated by the recent commissioning of high-frequency receivers at the Plateau de Bure interferometer (PdBI). In Section 2, we provide a brief overview of the new data and describe how their combination with previous SMA observations provides the sharpest view yet of the thermal emission from the LkCa 15 disk. In Section 3 we use simple models to explore the properties of the disk cavity and its contents. And in Section 4 we discuss those modeling results in the contexts of planet formation around LkCa 15 and the potential future utility of similar observations as an independent check on the properties of young exoplanets.

2. OBSERVATIONS AND DATA REDUCTION

LkCa 15 was observed for 5 hr with the most extended configuration (A: baselines of 130–760 m) of the PdBI on 2011 January 27. The observations were conducted in “shared-risk” mode since they used the new Band 4 receivers at an effective continuum frequency of 345.8 GHz (868 μm) and the new WideX correlator to sample the continuum emission with a total bandwidth of 3.6 GHz (per polarization). The observations cycled between LkCa 15 and two nearby quasars, J0530+1331 and J0336+3218, every 22 minutes. The data were calibrated with the CLIC software in the GILDAS package. Short observations of the bright quasars 3C 454.3 and 3C 273 were

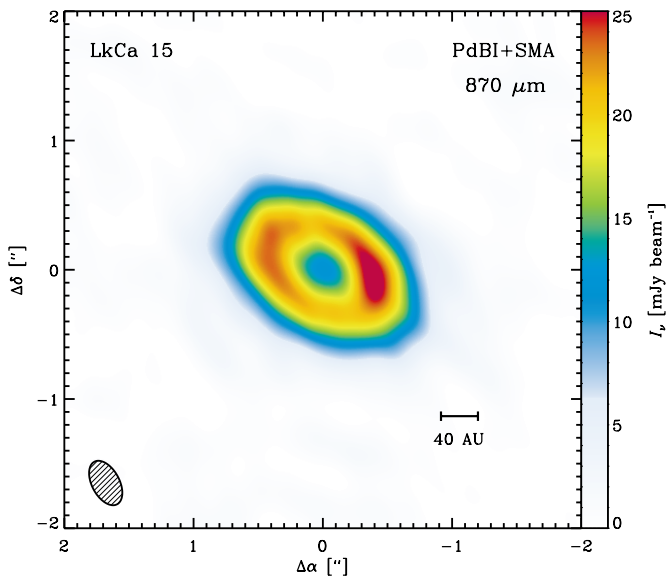


Figure 1. Aperture synthesis image of the $870\ \mu\text{m}$ continuum emission from the LkCa 15 disk, made from the naturally weighted combination of PdBI and SMA data sets. The synthesized beam, with dimensions of $0''.33 \times 0''.22$ (46×31 AU), is shown in the lower left. The wedge on the right marks the conversion from color to surface brightness. Each side of the image corresponds to 560 AU projected on the sky.

(A color version of this figure is available in the online journal.)

used to set the bandpass and absolute flux scale, and the nearby quasars that were interleaved in the observing cycle were utilized to calibrate the time-dependent complex gain response of the system. At the time of the observations, the new Band 4 LO system perturbed the first channel (of three) in the PdBI water vapor radiometer (WVR) phase correction system. We reduced the WVR system to a dual channel mode in the post-processing and smoothed the WVR data on 5 s intervals. The differential phase correction determined on 45 s intervals was extended over each source cycle by fitting and removing linear instrumental drifts. This process requires a stable atmosphere, with water vapor fluctuations that average to near zero over the source cycle. These conditions were generally met, due to the low water vapor levels (<2 mm) present throughout the observations.

To improve the Fourier coverage on short spacings, we supplemented these PdBI observations with the SMA data described by Andrews et al. (2011; baselines of 8–508 m). After adjusting the data sets to account for the small proper motion of LkCa 15 (Ducourant et al. 2005), the disk centroid was estimated in each data set by minimizing the imaginary components of the visibilities (see Andrews et al. 2011). The inferred reference centers for the two data sets agree within ~ 10 mas and are <70 mas from the expected stellar position (within the absolute astrometric uncertainty in each data set), at R.A. = $4^{\text{h}}39^{\text{m}}17^{\text{s}}.80$ and decl. = $+22^{\circ}21'03''.20$. The SMA and PdBI calibrations were compared over their redundant Fourier coverage, and were found to be in excellent agreement on 150–500 $\text{k}\lambda$ baselines: deviations between the visibility amplitudes in each data set are random, with an rms difference of $<5\%$. The combined SMA and PdBI visibilities were Fourier inverted assuming natural weighting, deconvolved with the CLEAN algorithm, and restored with a $0''.33 \times 0''.22$ synthesized beam using the MIRIAD software package. The resulting synthesized continuum map is shown in Figure 1, with an effective wavelength of $870\ \mu\text{m}$, rms noise of $0.7\ \text{mJy beam}^{-1}$, peak flux density of $27\ \text{mJy beam}^{-1}$, and integrated flux density of $380\ \text{mJy}$.

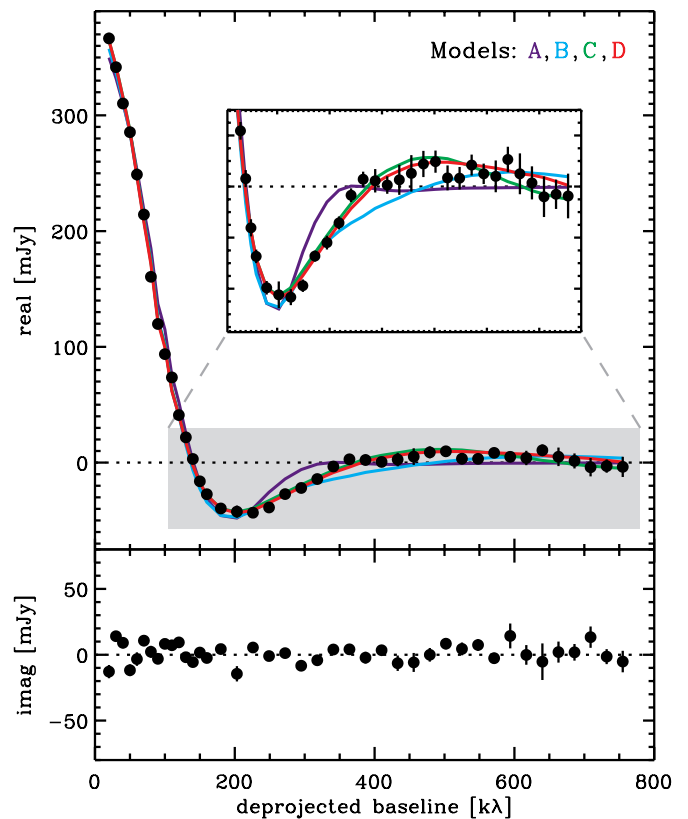


Figure 2. Real and imaginary $870\ \mu\text{m}$ visibilities as a function of baseline length, deprojected to account for the LkCa 15 disk viewing geometry and azimuthally averaged. The inset in the top panel is a detailed view of the gray-filled region. The best-fit models visibilities for different emission prescriptions are overlaid in color (all models have zero imaginary fluxes, by definition).

(A color version of this figure is available in the online journal.)

3. RESULTS

The $870\ \mu\text{m}$ image in Figure 1 provides the sharpest view yet of cool dust emission from the LkCa 15 disk. As noted previously at lower resolution (Piétu et al. 2006; Andrews et al. 2011), this emission has an inclined ring morphology with a large and prominent central depression in intensity. The emission ring peaks at semi-major separations of $\sim 0''.4$ (56 AU for an assumed distance of 140 pc) and has an aspect ratio and orientation in good agreement with the inclination ($i = 51^\circ$) and major axis position angle ($\text{PA} = 61^\circ$) inferred from its molecular line emission (Piétu et al. 2007). Figure 2 shows the azimuthally averaged visibilities as a function of the deprojected baseline length (accounting for the disk viewing geometry). The real part of this visibility profile exhibits the classic oscillation pattern expected from the Fourier transform of a ring in the sky-plane, with distinct nulls (sign changes) at deprojected baselines near 150, 350, and 700 $\text{k}\lambda$. The imaginary terms are negligible on all baselines, consistent with an axisymmetric emission distribution. Although subtle, two qualitative features in the data can serve as useful benchmarks in a refined effort to characterize the LkCa 15 disk structure. First, the continuum intensities inside the ring are small, but not zero (see Figure 1). And second, the oscillations in the continuum visibility profile are relatively muted, with a maximum amplitude of only ~ 5 mJy between the second and third nulls. This latter property suggests that the emission peak near the inner ring edge is not very sharp.

With those features in mind, we attempted to reproduce these LkCa 15 disk observations with simple $870\ \mu\text{m}$ emission

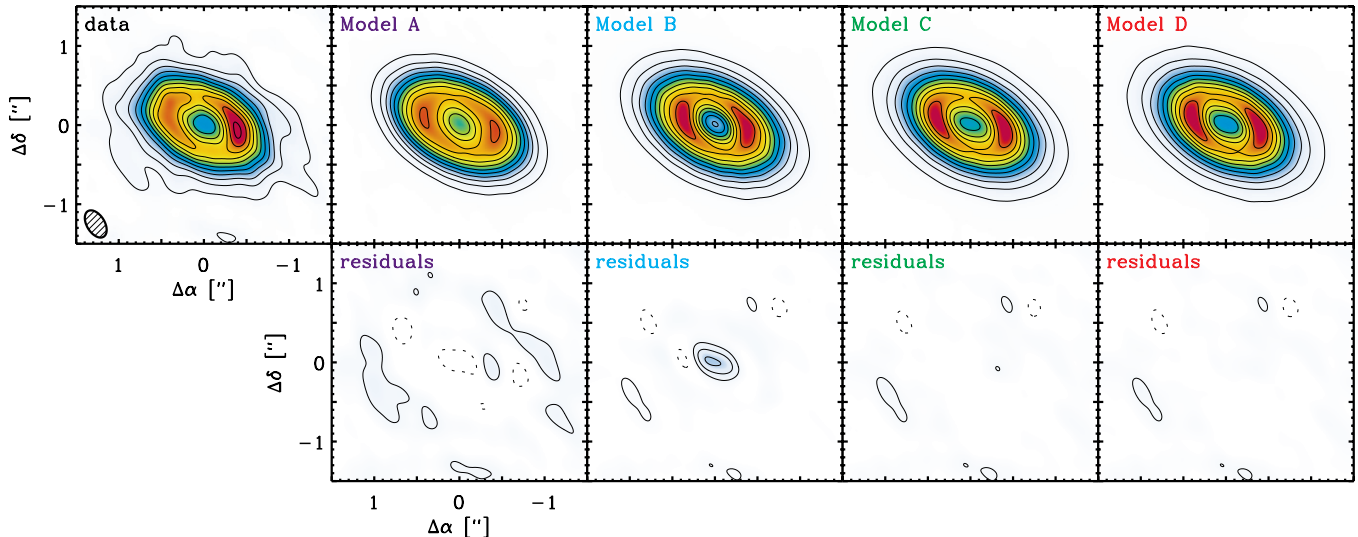


Figure 3. Comparison of the data and models in the image plane. The top left panel shows the same image as in Figure 1. To the right, the top panels display the best-fit model images and the bottom panels the imaged residual visibilities. All panels show the same color scale and contour levels, starting at $1.4 \text{ mJy beam}^{-1}$ (2σ) and increasing in $2.5 \text{ mJy beam}^{-1}$ (3.5σ) increments. As noted in Figure 2, Models C and D—which emulate a low-density (but not empty) cavity and a gap structure for the LkCa 15 disk, respectively—provide the best matches to the data.

(A color version of this figure is available in the online journal.)

Table 1
Model Parameters

Model	A	B	C	D
F_{tot} (mJy)	363 ± 2	373 ± 2	367 ± 3	385 ± 2
γ	-1.7 ± 0.1	-1.0 ± 0.1	-0.5 ± 0.1	-0.3 ± 0.1
R_c (AU)	107 ± 2	113 ± 1	114 ± 1	113 ± 1
R_{cav} (mJy)	...	36 ± 1	49 ± 1	...
δ	1 (fixed)	0 (fixed)	0.18 ± 0.02	...
R_s (AU)	16 (fixed)
q	0.009 ± 0.001
χ^2	516,735	516,600	516,489	516,484

Notes. Parameter estimates, formal uncertainties, and χ^2 values for the models discussed in Section 3. There are 776,966 independent visibilities used in the model fits.

models. We adopted a radial surface brightness prescription that assumes optically thin thermal emission, $I_v \propto B_v(T_d)(1 - e^{-\tau}) \approx B_v(T_d)\tau$, where B_v is the Planck function, T_d is the dust temperature, and τ is the optical depth. The temperature profile was fixed to $T_d(R) = 100(R/1 \text{ AU})^{-0.5}$ K, based on a crude approximation of the midplane temperatures derived in a more sophisticated treatment of radiative transfer (Andrews et al. 2011). Assuming that the dust emissivity is independent of radius, we utilized a parametric form for the base optical depth profile motivated by the surface densities in idealized viscous accretion disks: $\tau_b(R) \propto (R/R_c)^{-\gamma} \exp[-(R/R_c)^{2-\gamma}]$ (e.g., Hartmann et al. 1998). Modifications to that base model were also considered, including an optical depth cavity where $\tau(R \leq R_{\text{cav}}) = \delta\tau_b$. Three model permutations were investigated: the base model ($\delta = 1$, R_{cav} undefined; Model A), the base model with an empty cavity ($\delta = 0$; Model B), and the base model with a partially filled cavity ($0 < \delta < 1$; Model C). All models have three base parameters—a gradient (γ), characteristic size (R_c), and normalization (defined as the flux density, $F_{\text{tot}} = \int I_v d\Omega$)—and can utilize up to two additional parameters, $\{R_{\text{cav}}, \delta\}$.

For a given model type and parameter set, synthetic visibilities were computed for the appropriate viewing geometry

at the spatial frequencies observed by the SMA and PdBI. Those model visibilities were compared with the data and assigned a fit quality statistic, the sum of the (real and imaginary) χ^2 values over all spatial frequencies. The best-fit parameter values for a given model were determined by minimizing χ^2 with the Metropolis algorithm, utilizing multiple Monte Carlo Markov chains and an initial period of simulated annealing (see Gregory 2005). The results are compiled in Table 1. The estimated parameter uncertainties do not consider correlated errors from the (fixed) temperature profile or viewing geometry, and therefore are clearly underestimated. The best-fit synthetic data products for each model type are directly compared with the observations in Figures 2 and 3. The corresponding radial brightness profiles are shown together in Figure 4.

For Model A, the observed emission morphology can only be reproduced with a large and negative optical depth gradient parameter, γ (e.g., see Isella et al. 2009). The Model A fit does a relatively poor job accounting for the breadth of the observed ring structure: there is a tendency to overpredict the emission in the disk center and prematurely cut off at larger radii. Significant improvement is made with Model B, when a cavity is added to the base model. This is effectively the same structure assumed by Andrews et al. (2011). That preliminary work used a fixed $\gamma = 1$, which tends to maximize the peak-to-cavity emission contrast in the fits, leading to higher positive residuals at the disk center. Similar results were obtained when that effort was repeated here, with strong central residuals ($\sim 11\sigma = 8.2 \text{ mJy}$). The best-fit Model B parameters are different from the fixed-gradient case (see Table 1; $\chi_A^2 - \chi_B^2 = 135$)³—but those same residuals remain significant ($\sim 7\sigma = 4.8 \text{ mJy}$). Naturally, this motivated the addition of an emission component inside the disk cavity, cast for simplicity as an adjustment to δ (Model C). The inclusion of that weak emission improved the fit quality ($\chi_B^2 - \chi_C^2 = 111$), leaving no significant residuals compared to

³ The χ^2 differences in our progression of models are large enough (the best-fit likelihood ratios are significantly greater than unity) to warrant the complexity of adding a parameter at each step from Models A through C.

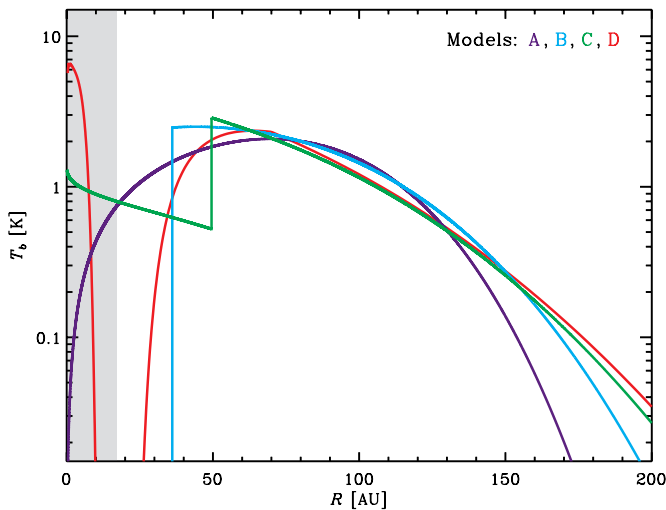


Figure 4. Radial surface brightness profiles for the best-fit parameters of each model type, cast for simplicity into a brightness temperature format. The combined PdBI+SMA data provide a maximum projected radial resolution of ~ 17 AU, marked here by the shaded gray region.

(A color version of this figure is available in the online journal.)

the data. In this scenario, dust inside the disk cavity produces ~ 5 mJy of $870 \mu\text{m}$ emission, corresponding to 20% of the peak surface brightness and only 1% of the integrated flux density.

A gap structure represents an alternative model that naturally produces dust emission inside a disk cavity. To explore that possibility with a more physically motivated prescription, we modeled the data with the treatment of gap profiles advocated by Crida et al. (2006) and Crida & Morbidelli (2007). In this scenario (Model D), we utilized a semi-analytic approximation for the surface density perturbation produced by an embedded low-mass companion to modify the base optical depth profile. The depth, width, and shape of the gap profile perturbation were characterized by Crida et al. (2006, their Equation (14)) in terms of the companion-to-star mass ratio ($q = M_s/M_*$), the semi-major axis of the companion (R_s), the disk viscosity (ν), and the local disk aspect ratio (H/R , where H is the vertical scale height of the gas). Following Crida and his colleagues, we fixed $H/R = 0.05$ and only investigated models where $\nu = 10^{-5}$ in the Crida et al. (2006) normalized units (for our fixed T_d profile, this corresponds to a typical viscosity coefficient $\alpha \sim 0.001$ in the formulation of Shakura & Sunyaev 1973). Furthermore, we fixed $R_s = 16$ AU, in line with the recent detection of a faint companion (Kraus & Ireland 2011; see Section 4). With these simplifying assumptions, Model D has four parameters, $\{\gamma, R_c, F_{\text{tot}}, q\}$. The Model D structure also has improved fit quality relative to the empty cavity model ($\chi_B^2 - \chi_D^2 = 116$, comparable to Model C). The estimate of q implies a companion mass of $M_s = 9 \pm 1 M_{\text{Jup}}$, given the LkCa 15 stellar mass of $M_* = 1.01 \pm 0.03 M_\odot$ that was determined dynamically by Piétu et al. (2007). We should again caution that these represent formal parameter uncertainty estimates that are only applicable under the restrained assumptions of this particular model; the true uncertainties could be significantly larger. As for Model C, there is roughly 5 mJy of $870 \mu\text{m}$ emission interior to the gap of the favored Model D structure.

4. DISCUSSION

We have used high angular resolution $870 \mu\text{m}$ PdBI+SMA observations to investigate the radial distribution of cool dust

in the LkCa 15 protoplanetary disk with simple emission models. Although grounded in more sophisticated techniques, these models are inherently more morphological than physical. Their advantage lies in computation speed, which facilitated a broader exploration of dust structures that would have been prohibitive for a complex radiative transfer analysis. Despite their limitations, these simple models provide some fundamental qualitative insights on the LkCa 15 disk properties: (1) there is a substantial decrease in the dust optical depths inside $R \approx 40\text{--}50$ AU; (2) the emission just outside that cavity edge is not sharply peaked, as attested by the smooth intensity profiles produced by the favored negative optical depth gradients (γ); and (3) there is a small amount of dust located inside the disk cavity. Given our limited resolution, the spatial distribution of that weak emission in the cavity is unclear. It may fill the cavity (Model C), or it may be more centrally concentrated in the form of a gap structure (Model D) similar to what was inferred from models of the unresolved infrared spectrum (Espaillat et al. 2008).

If the latter is true, the gap is most likely opened by the resonant torques generated by interactions between the disk and a low-mass companion (Lin & Papaloizou 1986; Bryden et al. 1999). Alternative gap-opening mechanisms—for example, photoevaporation—are unlikely given the properties of the LkCa 15 system (Alexander & Armitage 2009; Owen et al. 2011). High-contrast imaging has ruled out stellar and brown dwarf companions around LkCa 15, hinting that the gap may be opened by a young giant planet (Thalmann et al. 2010; Pott et al. 2010; Kraus et al. 2011). Recently, Kraus & Ireland (2011) used a non-redundant masking technique to detect a faint, comoving companion $\sim 0''.07$ from LkCa 15. If that object is co-planar with the disk and on a circular orbit, it has a semi-major axis of 16 AU. Using a simple emission model based on the prescription of Crida et al. (2006), we have shown that a gap at this location can reproduce well the resolved $870 \mu\text{m}$ emission morphology we observe if the companion mass is $\sim 9 M_{\text{Jup}}$. At ages of 1–3 Myr, the Baraffe et al. (2003) evolution models suggest that this object should have an infrared contrast of $\Delta K = 6.4\text{--}7.2$, in reasonable agreement with the $\Delta K = 6.8$ measured by Kraus & Ireland (2011). However, the Marley et al. (2007) models suggest it would be $\sim 150\times$ fainter: a substantial accretion luminosity would be required to account for the observed infrared emission.

Ultimately, improved constraints on the companion mass could be based on the disk contents interior to the gap. A crude estimate of the dust mass in that region can be made from the luminosity of the optically thin $870 \mu\text{m}$ emission that was inferred in Models C and D. Assuming a dust opacity of $3 \text{ cm}^2 \text{ g}^{-1}$ and a fiducial $T_d = 45$ K, the estimated flux density of 5 mJy corresponds to $10^{-6} M_\odot$ ($0.4 M_\oplus$). If that dust traces the gas at a mass fraction of $\sim 1\%$, then the accretion rate onto LkCa 15 ($\dot{M}_* \approx 2 \times 10^{-9} M_\odot \text{ yr}^{-1}$; Ingleby et al. 2009) implies that this inner disk material would rapidly drain onto the star (in < 0.05 Myr). Given the system age of 1–3 Myr, the inner disk must be continually replenished from the massive reservoir outside the gap. There is some notable tension with theoretical expectations here: it is not clear how a $\sim 9 M_{\text{Jup}}$ companion can be reconciled with the inferred inner disk mass and stellar accretion rate in numerical simulations of gap-crossing flows (Lubow et al. 1999; Lubow & D’Angelo 2006). If LkCa 15b has a much lower mass, it likely cannot sculpt the deep, wide gap needed to explain the observations; an additional companion with a longer orbital period must also be present. Zhu et al.

(2011) and Dodson-Robinson & Salyk (2011) have effectively argued for this latter possibility. They suggested that multi-planet systems can alleviate the apparent discrepancy between large transition disk cavities and accretion rates, implying that LkCa 15b is but one component in a young planetary system.

Robust, quantitative constraints on the properties of LkCa 15b based on the structure of the LkCa 15 disk require more work, including a stronger link between numerical simulations, an improved modeling effort, and observations that can probe the inner disk at even higher angular resolution. Nevertheless, the PdBI+SMA data presented here offer a tantalizing foreshadowing of the new roles millimeter-wave observations of disk structures can play in exoplanet science.

We are very grateful to Adam Kraus for his advice and for kindly sharing results prior to publication. This article is based on observations carried out with the IRAM Plateau de Bure Interferometer and the Submillimeter Array. IRAM is supported by INSU/CNRS (France), MPG (Germany), and IGN (Spain). The SMA is a joint project between the Smithsonian Astrophysical Observatory and the Academia Sinica Institute of Astronomy and Astrophysics and is funded by the Smithsonian Institution and the Academia Sinica.

REFERENCES

- Alexander, R. D., & Armitage, P. J. 2009, *ApJ*, 704, 989
- Andrews, S. M., Wilner, D. J., Espaillat, C., et al. 2011, *ApJ*, 732, 42
- Baraffe, I., Chabrier, G., Barman, T. S., Allard, F., & Hauschildt, P. H. 2003, *A&A*, 402, 701
- Bryden, G., Chen, X., Lin, D. N. C., Nelson, R. P., & Papaloizou, J. C. B. 1999, *ApJ*, 514, 344
- Crida, A., & Morbidelli, A. 2007, *MNRAS*, 377, 1324
- Crida, A., Morbidelli, A., & Masset, F. 2006, *Icarus*, 181, 587
- Dodson-Robinson, S. E., & Salyk, C. 2011, *ApJ*, 738, 131
- Ducourant, C., Teixeira, R., Périé, J. P., et al. 2005, *A&A*, 438, 769
- Espaillat, C., Calvet, N., D'Alessio, P., et al. 2007, *ApJ*, 670, L135
- Espaillat, C., Calvet, N., Luhman, K. L., Muzerolle, J., & D'Alessio, P. 2008, *ApJ*, 682, L125
- Gregory, P. C. 2005, *Bayesian Logical Data Analysis for the Physical Sciences: A Comparative Approach with Mathematica Support* (Cambridge: Cambridge Univ. Press)
- Hartmann, L., Calvet, N., Gullbring, E., & D'Alessio, P. 1998, *ApJ*, 495, 385
- Huélamo, N., et al. 2008, *A&A*, 489, L9
- Ida, S., & Lin, D. N. C. 2004, *ApJ*, 604, 388
- Ingleby, L., et al. 2009, *ApJ*, 703, L137
- Isella, A., Carpenter, J. M., & Sargent, A. I. 2009, *ApJ*, 701, 260
- Kraus, A. L., & Ireland, M. J. 2011, *ApJ*, in press (arXiv:1110.3808)
- Kraus, A. L., Ireland, M. J., Martinache, F., & Hillenbrand, L. A. 2011, *ApJ*, 731, 8
- Lin, D. N. C., & Papaloizou, J. 1986, *ApJ*, 309, 846
- Lubow, S. H., & D'Angelo, G. 2006, *ApJ*, 641, 526
- Lubow, S. H., Seibert, M., & Artymowicz, P. 1996, *ApJ*, 526, 1001
- Marley, M. S., Fortney, J. J., Hubickyj, O., Bodenheimer, P., & Lissauer, J. J. 2007, *ApJ*, 655, 541
- Mordasini, C., Alibert, Y., & Benz, W. 2009, *A&A*, 501, 1139
- Owen, J. E., Ercolano, B., & Clarke, C. J. 2011, *MNRAS*, 412, 13
- Piétu, V., Dutrey, A., & Guilloteau, S. 2007, *A&A*, 467, 163
- Piétu, V., Dutrey, A., Guilloteau, S., Chapillon, E., & Pety, J. 2006, *A&A*, 460, L43
- Pott, J.-U., Perrin, M. D., Furlan, E., et al. 2010, *ApJ*, 710, 265
- Quillen, A. C., Blackman, E. G., Frank, A., & Varnière, P. 2004, *ApJ*, 612, L137
- Shakura, N. I., & Sunyaev, R. A. 1973, *A&A*, 24, 337
- Thalmann, C., et al. 2010, *ApJ*, 718, L87
- Varnière, P., Blackman, E. G., Frank, A., & Quillen, A. C. 2006, *ApJ*, 640, 1110
- Zhu, Z., Nelson, R. P., Hartmann, L., Espaillat, C., & Calvet, N. 2011, *ApJ*, 729, 47